Regular Article

PHYSICAL CHEMISTRY RESEARCH
Published by the
Iranian Chemical Society
www.physchemres.org
info@physchemres.org

Phys. Chem. Res., Vol. 11, No. 4, 837-851, December 2023
DOI: 10.22036/pcr.2022.365267.2219

Interaction of Electronically Excited CO($a^3\Pi_r$) Molecules with H, H_2, and H_2O: Potential Energy Surfaces and Reaction Kinetics

A.V. Pelevkin, B.I. Loukhovitski and A.S. Sharipov*
Central Institute of Aviation Motors, Moscow 111116, Russia
(Received 17 October 2022, Accepted 26 November 2022)

The kinetics of elementary reactions of H, H_2, and H_2O species with electronically excited CO (triplet Π state) was theoretically studied using the multireference second-order perturbation theory. The corresponding thermodynamically and kinetically favored reaction pathways were identified. It was found that the reactivity of the CO($a^3\Pi_r$) molecule to the above small H-containing species was much higher than that of the ground-state CO($X^1\Sigma^+$) molecule. Appropriate thermal rate constants for the specified reaction channels with CO($a^3\Pi_r$) were obtained using the Rice-Ramsperger-Kassel-Marcus/master equation calculations and adiabatic approximation. The obtained temperature-dependent rate coefficients can be incorporated into the future kinetic sub-mechanisms aimed to describe the ultraviolet CO($a^3\Pi_r - X^1\Sigma^+$) flame chemiluminescence. The corresponding Arrhenius-type expressions are reported for a wide temperature range (T = 200-3000 K), relevant to both atmospheric and combustion chemistry.

Keywords: Carbon monoxide, Excited states, Elementary processes, Quantum chemistry, Chemiluminescence, Combustion diagnostics

INTRODUCTION

It is generally accepted that visible and ultraviolet (UV) flame chemiluminescence, as optical signatures of the combustion process [1-2], can readily be used for non-intrusive combustion diagnostics [3-6]. Since the spectrometry of spontaneous emission from chemiluminescent species does not require an external radiation source and hence not expensive laser instrumentation, the analysis of emission spectra from reacting flows is somehow a cheap and practical alternative to the laser-based flame diagnostics tools [4-8]. It must be noted that for hydrocarbon-air flames, the major emitters are the electronically excited radicals OH*, CH*, and C_2* (hereafter, the asterisk denotes an electronically excited state).

Although chemiluminescence, arising from minor excited-state species, *per se* does not directly provide basic information on flame chemistry, the kinetics of formation and consumption of radiating components is closely related to the abundance of key atomic species and radicals that govern the combustion chemistry (so-called *chain carriers* [9]). Therefore, proper quantitative interpretation of spatially and spectrally resolved chemiluminescence can provide insight into the flame structure [3-8].

Whereas chemiluminescence diagnostics of combustion is usually focused on the emission spectra of OH*, CH*, and C_2* excited species [3-8], for a number of carbonaceous combustible mixtures characterized by excess atomic oxygen during the ignition period, the data on the flame structure can be significantly supplemented by analyzing the middle and far UV Cameron band emission [10] from an electronically excited CO* molecule [11-16] (specifically, metastable $a^3\Pi_r$ state with energy relative to the ground $X^1\Sigma^+$ state T_e = 6.01 eV [17] and a radiative lifetime of 4 ÷ 5 ms [16, 18]). It is worth noting in this connection that, the intensity of CO* chemiluminescence increases with the temperature of the gas mixture; thus, the analysis of the corresponding

*Corresponding author. E-mail: aleksandr.sharipov@phystech.edu

emission spectra can provide important information on not only the kinetics of high-temperature combustion of various carbonaceous fuels [14,16] but also the processes involved in high-enthalpy gas flows containing CO [19-22].

In fact, to arrive at a reliable quantitative interpretation of CO* emission measurements, it is necessary to develop kinetic models that can describe the production and consumption of excited CO* molecules (mainly $a^3\Pi_r$, and, to a lesser extent, $A^1\Pi$ state [11-12]) under combustion conditions, but until very recently, there have been actually no such models. The development of such models is obviously hampered by the fragmentary nature of the known data on elementary processes involving CO*.

Nevertheless, in recent years, due to the advantages in CO* chemiluminescence diagnostics of high-temperature combustion [16] and in an attempt to further our understanding of the chemistry of excited electronic states under strongly non-equilibrium conditions relevant to post-shock flows [20-21,23] and electric discharge plasma [24-30], more and more submodels have started to be developed to describe electronically excited CO* molecules [16,28-30]. These sub-models can be incorporated into conventional chemical reaction mechanisms describing the evolution of the ground-state species. The design and further refinement of such sub-mechanisms will increase the accuracy of non-intrusive CO* emission spectroscopy techniques for combustion diagnostics [16] and improve the prediction of the radiation heat flux from shock- [20-21] and discharge-heated [24,30] gas flows. In addition, these sub-mechanisms can be used to assess the effect of super-equilibrium CO* abundance, maintained by means of electric discharge with a relatively high reduced electric field [27,30], on the intensification of chain processes in the CO-containing reactive mixtures with reference to the problems of plasma-assisted combustion [31] and plasma processing [28-30]. Finally, the increasing importance of CO* chemiluminescence in extraterrestrial atmospheric photochemistry [32-35] and UV astronomy [34,36] has encouraged more researchers to conduct theoretical (both semiempirical and *ab initio*) studies on the elementary processes involving electronically excited CO molecules [16, 25,37-41]. Meanwhile, it should be recognized that the treatment of the reactivity of excited electronic states continues to be a challenge to the present quantum chemical methods [40,42-47].

While the basic reaction sub-mechanism (*i.e.*, the set of elementary reactions together with the corresponding rate constants) describing the kinetics of CO($a^3\Pi_r$) in the thermal non-equilibrium CO-CO_2 mixture is now generally established, mainly aiming at discharge chemistry [28-30], it is certainly insufficient to describe the CO* chemiluminescence from hydrocarbon and CO-containing flames. In view of the fact that elementary chemical reactions involving the simplest H-containing species (H, H_2, and H_2O) underlie the oxidation kinetics of any hydrocarbon and synthetic fuels [8-9], the data on the reactivity of CO($a^3\Pi_r$) to such hydrogenous species are of paramount importance in describing the accompanying CO* chemiluminescence due to CO($a^3\Pi_r - X^1\Sigma^+$) transitions in flames (at a wavelength of around 216 nm) [16,31]. However, as far as the authors are aware, there are no reliable estimates of the corresponding rate constants, apart from those provided by Zanchet *et al.* using the *ab initio*-based quasi-classical trajectory (QCT) method [37] for some channels of the CO($a^3\Pi_r$) + H reaction and those essentially semiempirical assessments provided by the authors in their proceeding work for the reaction of CO($a^3\Pi_r$) with molecular hydrogen [16].

In the absence of any relevant experimental observations, the above points highlight the need for a detailed quantum chemical analysis of kinetic processes involved in the CO($a^3\Pi_r$) + H, CO($a^3\Pi_r$) + H_2, and CO($a^3\Pi_r$) + H_2O reacting systems. The present study aimed at addressing this gap in the literature.

METHODOLOGY

In the present study, a series *ab initio* quantum chemical calculations were performed for the reactions of ground-state H, H_2, and H_2O species with CO molecule, lying either in the ground $X^1\Sigma^+$ or the first excited $a^3\Pi_r$ electronic state, to examine the potential energy surfaces (PESs) and analyze the relevant reaction pathways. As a preferred computational workhorse, the state-averaged complete active space self-consistent field (CASSCF) method [48] with flat weighting for the states under investigation [43,49] was utilized, followed by the extended multi-configuration quasi-degenerate second-order perturbation theory (XMCQDPT2) [50] calculations based on the CASSCF wave

function as the reference state. This combination enabled the researchers to explore both the ground and excited PESs of interest on a unified basis and include dynamic electron correlation, which is clearly missing in the CASSCF calculations [45,51]. It is believed that the use of such multireference electron correlation treatment can improve the accuracy of reaction barrier heights [40,45,52-56] and excited-state geometries [56-57] so that they are comparable to those provided by highly correlated electronic structure methods.

Following the literature [43,58], the so-called *full-valence* active space was used for the CO + H and CO + H_2 systems. That is, in the first case, the active space consisted of 11 electrons distributed in 9 active orbitals [conventionally denoted as (11,9)] while in the second case, it comprised 12 electrons and 10 orbitals [denoted as (12,10)]. At last, the active space for the CO + H_2O system was built with 14 electrons in 12 active orbitals (14,12).

The diffuse-augmented Dunning's correlation consistent quadruple-zeta basis set aug-cc-pVQZ [59], as a reasonable approximation for the complete basis set limit on the excited PESs of small and medium-sized reactive systems [60-61], was applied throughout this study.

For ease of reference, hereafter, in the used *ab initio* model denoted as XMCQDPT2(*N*,*M*)/aug-cc-pVQZ, *N* and *M* refer to the numbers of electrons and orbitals in the active space. All electronic structure calculations were performed using the Firefly QC package [62] partially based on the GAMESS (US) source code [63].

The spatial structures of the reactants, transition states (TS), intermediates (IM), and reaction products on the considered PESs were optimized using the XMCQDPT2 method and the numerical gradients based on equidistant second-order central finite differences.

To verify the number of imaginary frequencies (the only imaginary frequency indicates the TS) for all the located critical points on the PES and, at the same time, compute the zero-point energy (ZPE) contribution to their energetics, a harmonic vibrational frequency analysis was employed using the same computational model as applied for optimization. For each of the TS identified, the corresponding minimum energy (steepest descent) path (MEP) was calculated using mass- weighted intrinsic reaction coordinates in both directions applying the Gonzalez-Schlegel integration method [64].

Finally, it should be noted that a systematic search for intersystem crossings, responsible for the nonadiabatic and electronic energy-transfer processes, remained outside the scope of this work, yet it would be desirable if future studies take this point into account for more accurate reaction rate constant calculations.

RESULTS AND DISCUSSION

Potential Energy Surfaces and Reaction Pathways

The calculation results for reaction pathways, which connect the reactants and products of CO($X^1\Sigma^+/a^3\Pi_r$) + H, CO($X^1\Sigma^+/a^3\Pi_r$) + H_2, and CO($X^1\Sigma^+/a^3\Pi_r$) + H_2O processes, are schematically depicted in Figs. 1, 2, and 3, respectively. Hereafter, the following designations are used for critical points (TSs and IMs): The left superscript denotes the spin multiplicity, and the right subscript refers to the order number (within the specific PES diagram) of a given critical point among those of the same spin multiplicity.

Energy values, spatial structures, harmonic frequencies of normal vibrations, and rotational constants for reactants, products, saddle points, and local minima are provided as Supplementary material. The energies of critical points corrected for corresponding ZPE values are summarized in Tables 1, 2, and 3.

In what follows, each of the obtained reaction diagrams is presented and explained in detail.

Interaction of CO($a^3\Pi_r$) with H

The PES diagram for the two lowest electronic states of the CO + H system, obtained at the XMCQDPT2(11,9)/aug-cc-pVQZ level of theory, is displayed in Fig. 1. As can be seen in Fig. 1, the reaction dynamics in this seemingly simple triatomic system (*i.e*., CO + H) is quite complex, even without considering the possible electronic excitation of CO. In particular, the CO($X^1\Sigma^+$) + H addition path on the lowest doublet (ground) PES produces either the ground state formyl radical HCO(X^2A') ($^2IM_0$, when applying the notation adopted in Fig. 1), through a low-lying transition state $^2TS_0$, or its metastable isomer COH($^2IM_1$) *via* a higher-lying $^2TS_1$ structure. Then, the COH component (isoformyl) can isomerize into HCO (*via* $^2TS_2$) or dissociate toward C + OH with no potential energy barrier above the reaction endoergicity.

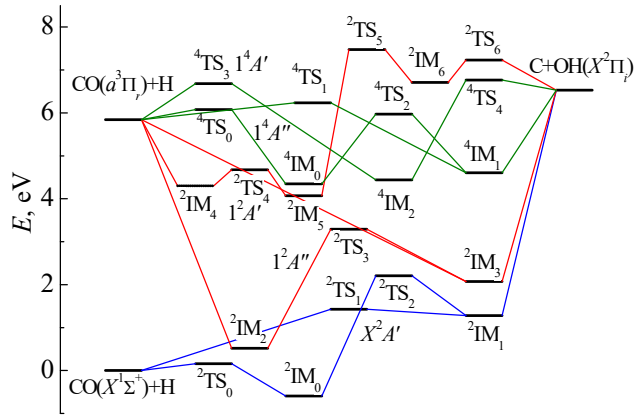

Fig. 1. The doublet and quartet electronic terms considered for the CO + H system calculated with ZPE correction.

In general, the results presented in Fig. 1 for the non-degenerate doublet PES correlating with the ground state bimolecular reactants and HCO(X^2A') radical were qualitatively and quantitatively consistent with those of previous relevant studies [65-70], including those obtained using high-level methods [67-70]. These results do not add anything particularly new to the existing knowledge on the subject. Moreover, the energies (relative to reactants) obtained for critical points on the lowest doublet PES during the multireference calculations were quite similar to those obtained from the accurate *ab initio* calculations [67-69] and Active Thermochemical Tables (ATcT) [71] (see Table 1), which indicates the relevance of the selected methodology in the present study. In particular, the entrance energy barrier obtained for the CO($X^1\Sigma^+$) + H reaction (0.156 eV) was well within the 0.06-0.20 eV range calculated elsewhere [67-69] by MRCI and CCSD(T) methods.

The calculated endoergicity of the CO($X^1\Sigma^+$) + H → C + OH reaction (6.531 eV) was also in reasonable accord with that recently found by Albernaz *et al.* [68] at the CCSD(T)/aug-cc-pVQZ level of theory (6.486 eV) and that estimated based on the ATcT [71] (6.700 eV). Our findings regarding the two excited doublet and two quartet PESs, which correlated with the electronically excited reactants CO($a^3\Pi_r$) + H [originated from the twofold orbital degeneracy of CO in an Π electronic state and, respectively, fourfold orbital degeneracy of CO($a^3\Pi_r$) + system], revealed something new. To Going into detail, in Zanchet *et al.'s* [37-38] studies, in which the above reaction system was investigated starting from the exit channel to C + OH products, the reaction

Table 1. A Comparison of the Energy Values of Critical Points with Respect to the Ground State Reagents for the CO + H System Obtained in This Work and Elsewhere (in eV)

Structure	This work	Previous studies	Method	Ref.
$^2TS_0$	0.156	0.197	MRCI+Q	[67]
		0.058	CCSD(T)	[68]
		0.160	CCSD(T)	[69]
$^2IM_0$	-0.596	-0.579	MRCI+Q	[67]
		-0.833	CCSD(T)	[68]
		-0.625	CCSD(T)	[69]
		-0.631	ATcT	[71]
$^2TS_1$	1.425	1.389	CCSD(T)	[68]
$^2TS_2$	2.206	2.037	CCSD(T)	[68]
$^2IM_1$	1.279	0.937	CCSD(T)	[68]
		1.192	ATcT	[71]
C + OH	6.531	6.486	CCSD(T)	[68]
		6.700	ATcT	[71]
CO($a^3\Pi_r$) + H	5.840	6.010	spectrosc.	[17]
		6.050	MR-SDCI	[37]
$^2IM_2$	0.518	0.30	MR-SDCI	[37]
$^2TS_3$	3.292	3.25	MR-SDCI	[37]
$^2IM_3$	2.072	1.83	MR-SDCI	[37]
$^2IM_4$	4.3[a]			
$^2TS_4$	4.677			
$^2IM_5$	4.069			
$^2TS_5$	7.476			
$^2IM_6$	6.712			
$^2TS_6$	7.233			
$^4TS_0$	6.076	6.35	MR-SDCI	[37]
$^4IM_0$	4.350	4.21	MR-SDCI	[37]
$^4TS_2$	5.971	6.13	MR-SDCI	[37]
$^4IM_1$	4.605	4.61	MR-SDCI	[37]
$^4TS_1$	6.234	6.49	MR-SDCI	[37]
$^4TS_3$	6.684			
$^4IM_2$	4.441			
$^4TS_4$	6.767			

[a]The optimization did not converge using default convergence criteria (see text); instead, the rough estimate obtained with the relaxed convergence requirements is provided.

pathways *via* the $^2TS_4$-$^2TS_5$-$^2TS_6$ and $^4TS_3$-$^4TS_4$ cascades of successive saddle points were not identified. In the present study, however, we managed to identify the $^2TS_4$ transition state at the XMCQDPT2(11,9)/aug-cc-pVQZ level of theory, but due to the divergence problem in CASSCF calculations using the same method, we were unable to reliably locate the $^2IM_4$ minimum.

Analogous with the ground PES, the relative energy values obtained in this study for the critical points on the excited PESs were quite similar to those reported by Zanchet *et al.* [37] using multireference calculations and those of spectroscopic data [17] (see Table 1). We note, in passing, that the energy spacing between the excited and ground-state PESs in the reactant region, which is nothing but the electronic excitation energy T_e of CO($a^3\Pi_r$) molecule, was found to be less than 3% different from the spectroscopic value of 6.01 eV [17]. In general, the dynamics of the CO($a^3\Pi_r$) + H process were observed to be extremely complex, and, as our preliminary research of PES intersections showed, the accurate evaluation of the corresponding rate constants is impossible without allowance for probable intersystem conversion.

Interaction of CO($a^3\Pi_r$) with H_2

The PES diagram for the two lowest electronic states of the CO + H_2 system, obtained at the XMCQDPT2(12,10)/aug-cc-pVQZ level of treatment, is shown in Fig. 2. The relative energies with respect to reactants for the critical points on these PESs, compared to the reference values based on the prior theoretical calculations [72-75], ATcT thermochemical database [71], and the compendium of electronic energy levels of polyatomic transient molecules [76], are presented in Table 2.

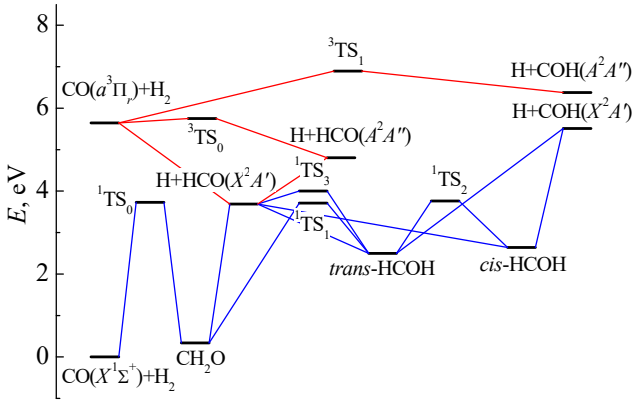

Fig. 2. The singlet and triplet electronic terms considered for the CO + H_2 system calculated with the ZPE correction.

Table 2. A Comparison of the Energy Values of Critical Points with Respect to the Ground State Reagents for the CO + H_2 System Obtained in the Present Work and Elsewhere (in eV)

Structure	This study	Previous studies	Method	Ref.
$^1TS_0$	3.730	3.553	CCSD(T)	[72]
		3.591	MRCI	[73]
		4.147	CASSCF	[74]
		3.581	CCSD(T)	[75]
CH_2O	0.337	-0.239	CCSD(T)	[72]
		0.087	ATcT	[71]
		-0.150	MRCI	[73]
		1.049	CASSCF	[74]
		0.105	CCSD(T)	[75]
H + HCO($^2A'$)	3.687	3.882	CCSD(T)	[72]
		3.848	ATcT	[71]
		3.968	MRCI	[73]
		3.973	CASSCF	[74]
		3.857	CCSD(T)	[75]
$^1TS_1$	3.713	3.498	CCSD(T)	[72]
		3.671	CCSD(T)	[75]
trans-HCOH	2.499	1.990	CCSD(T)	[72]
		2.105	MRCI	[73]
		2.352	CCSD(T)	[75]
$^1TS_2$	3.760	3.150	CCSD(T)	[72]
		3.404	MRCI	[73]
cis-HCOH	2.640	2.181	CCSD(T)	[72]
		2.305	MRCI	[73]
H + COH($^2A'$)	5.510	5.671	ATcT	[71]
		5.668	CCSD(T)	[75]
$^1TS_3$	4.002			
CO($a^3\Pi_r$) + H_2	5.644	6.010	Spectrosc.	[17]
$^3TS_0$	5.752			
H + HCO($^2A''$)	4.803	5.001	ATcT+spectr.	[71, 76]
$^3TS_1$	6.893			
H + COH($^2A''$)	6.379			

The PES obtained for the $CO(X^1\Sigma^+)$ + H_2 system in the present study largely coincided with those of previous studies [72-75,77]. Thus, it can be stated that the reaction of $CO(X^1\Sigma^+)$ with H_2 leads to the formation of a monomolecular product, *i.e.*, formaldehyde CH_2O, through the saddle point $^1TS_0$ (based on the notation used in Fig. 2), with an energy barrier of about 3.6 ÷ 4.2 eV [72-75]. It is worth mentioning that the barrier height obtained for this process in the present work (3.73 eV) was clearly within the above range. The CH_2O molecule, in turn, can alternatively isomerize into *cis* and *trans* forms of HCOH or dissociate to H and $HCO(X^2A')$ (formyl radical) with no energy barrier above the reaction endothermicity. Moreover, the relative energies obtained in the present study for critical points on the singlet PES were quite similar to those reported in previous studies [72-75] and calculated using the ATcT thermochemical data [71].

As for the $CO(a^3\Pi_r)$ + H_2 reacting system, $CO(a^3\Pi_r)$ directly interacts with H_2 (*i.e.*, the reaction bypasses the formation of an intermediate collision complex) via the twofold orbital degeneracy of carbon monoxide in the triplet Π state, along two different triplet PESs, resulting in the formation of either ground-state bimolecular products H + $HCO(X^2A')$ or electronically excited H + $HCO(A^2A'')$ (*via* $^3TS_0$) and H + $COH(A^2A'')$ (*via* $^3TS_1$) radical pairs. In the first case, as can be seen in Fig. 2, the reaction pathway is barrierless, as opposed to the counterpart process with the ground state CO molecule. Therefore, this channel is expected to prevail over other reactions with apparently little (at least, at not very high temperatures) chemical significance, leading to the formation of excited formyl and isoformyl *via* $^3TS_0$ and $^3TS_1$.

Our findings showed the absence of a direct minimum-energy path, from the reactants to any monomolecular product (*e.g.*, formaldehyde in the triplet electronic state), on the triplet PES, in contrast to the singlet PES, which is also supported by the findings of previous studies [44].

Interaction of $CO(a^3\Pi_r)$ with H_2O

The PES diagram for the two lowest electronic states of the CO + H_2O system, based on the XMCQDPT2 (14,12)/aug-cc-pVQZ calculations, is plotted in Fig. 3. The energies of the critical points on these PESs with respect to reactants, compared to the reference values based on the previous theoretical studies [78-80] and available databases [71,76], are listed in Table 3.

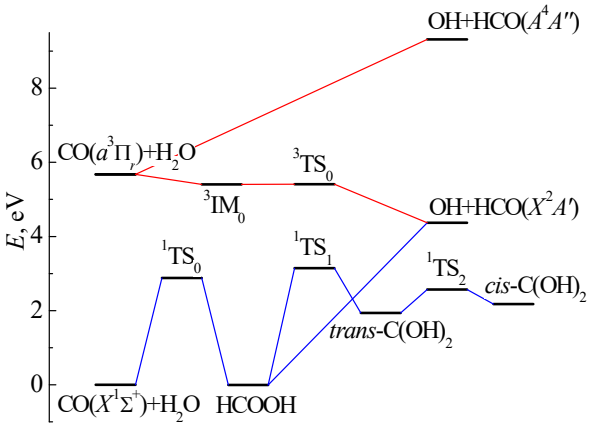

Fig. 3. The singlet and triplet electronic terms considered for the CO + H_2O system calculated with the ZPE correction.

Table 3. The Energy Values of Critical Points with Respect to the Ground State Reagents for the CO + H_2O System Obtained in This Work and Elsewhere (in eV)

Structure	This study	Previous studies	Method	Ref.
$^1TS_0$	2.880	2.919	CCSD(T)	[78]
		2.713	CCSD(T)	[79]
		2.754	CCSD	[80]
HCOOH	-0.003	-0.157	CCSD(T)	[79]
		-0.386	CCSD	[80]
		-0.190	ATcT	[71]
$^1TS_1$	3.148	3.095	CCSD(T)	[79]
trans-C(OH)$_2$	1.935			
$^1TS_2$	2.571			
cis-C(OH)$_2$	1.935			
OH + $HCO(^2A')$	4.369	4.399	CCSD(T)	[79]
		4.471	ATcT	[71]
$CO(a^3\Pi_r)$ + H_2O	5.677	6.010	Spectrosc.	[17]
$^3IM_0$	5.403			
$^3TS_0$	5.412			
OH + $HCO(^4A'')$	9.314	8.319	ATcT+spectr.	[71, 76]

The reaction of CO($X^1\Sigma^+$) with H_2O was found to proceed *via* the saddle point $^1TS_0$ (using the notation in Fig. 3) on the singlet (ground) PES, leading to the formation of formic acid HCOOH, which, in turn, can isomerize or dissociate to OH + HCO(X^2A'). These findings are basically consistent with those reported in previous studies for this singlet PES [78-80]. For instance, to initiate the reaction between CO($X^1\Sigma^+$) and H_2O, at least 2.88 eV energy is required, and the barrier height obtained in this study was in good agreement with this data [78-80].

As for the CO($a^3\Pi_r$) + H_2O reacting system, the interaction between CO($a^3\Pi_r$) with H_2O occurred *via* the twofold orbital degeneracy of carbon monoxide in the triplet Π state, along two different triplet PESs, resulting in the formation of either the ground-state [OH + HCO($^2A'$)] or the excited-state [OH + HCO($^4A''$)] bimolecular products. In the former case, the reaction is initiated by a shallow pre-reaction van der Waals complex $^3IM_0$ without an entrance barrier. However, since the subsequent $^3TS_0$ saddle point stands lower than CO($a^3\Pi_r$) + H_2O in terms of energy, the overall reaction, as opposed to the counterpart route with the ground state CO molecule, is barrier-free. Concerning the possibility of OH + HCO($^4A''$) formation, it did not appear to be of chemical significance for the title reaction due to the very high excitation energy of the HCO($^4A''$) molecule (T_e = 5.02 eV [37]). This pathway may be relevant only in the kinetics of electronically excited HCO states *per se*.

Reaction Kinetics

As it follows from the above analysis, for the reacting systems considered in this study, the following principal reaction channels involving CO($a^3\Pi_r$) can be recommended for inclusion in future sub-mechanisms aimed to describe the CO($a^3\Pi_r - X^1\Sigma^+$) flame chemiluminescence:

$$CO(a^3\Pi_r) + H \rightarrow C + OH \quad (R1)$$

$$CO(a^3\Pi_r) + H_2 \rightarrow H + HCO(X^2A') \quad (R2)$$

$$CO(a^3\Pi_r) + H_2O \rightarrow OH + HCO(X^2A') \quad (R3)$$

Other identified channels, in particular those leading to the stabilization of electronically excited intermediates and formation of electronically excited bimolecular products, can hardly be included in the kinetic models under development due to the lack of data on other reactions with these energized species.

Based on the diagrams provided above in Figs. 1, 2, and 3, it can be stated that the energy barriers of R1, R2, and R3 reaction channels were much lower than those of the counterpart processes with the ground state carbon monoxide. The CO($X^1\Sigma^+$) + H → C + OH process is designated hereafter as R0 for convenience; in addition, the minus sign is used to indicate a backward reaction. Accordingly, the excited CO($a^3\Pi_r$) molecule must have extremely high reactivity to H, H_2, and H_2O species, which is not particularly surprising given the rather high energy of the $a^3\Pi_r$ excited state relative to that of the ground $X^1\Sigma^+$ state and the intuitive idea that electronic excitation basically reduces the reaction barriers [81]. Despite the fact that the analysis of PESs was quite detailed in the present study, the reported barrier heights and TS properties (listed in Supplementary material) alone are not enough for the kinetic modeling of CO* evolution; therefore, it is recommended that the corresponding rate constants be further evaluated.

Nevertheless, the precise calculation of rate constants goes beyond the intent of the present work because, in particular, it is very difficult to calculate such rate constants for the complex-mediated R1 process due to the need for consistent treatment of (*i*) the formation/decay of collision complexes ($^2IM_4$, $^2IM_5$, $^2IM_6$, $^4IM_0$, $^4IM_1$, and $^4IM_2$) and (*ii*) nonadiabatic coupling between different PESs. Since the second of the mentioned aspects was not considered in this study, the best that could be done to estimate the R1 rate constant was to conduct Rice-Ramsperger-Kassel-Marcus (RRKM) theory-based master equation (ME) analysis [82-83], neglecting the possibility of electronically nonadiabatic transitions. Thus, based on the obtained geometries, vibrational frequencies, and relative energies of the reactants, products, intermediates, and transition states, phenomenological rate constants were estimated for R1 and R3 reactions at various temperatures (T = 200-3000 K) and pressures (P = 10^{-2}-10^2 bar) using the RRKM-ME theoretical approach, as implemented in the MESS package [84,85]. In doing so, the required densities of states and partition functions for local minima and transition states were conventionally calculated under the rigid-rotor/harmonic-oscillator approximation [83]. Then, the simple exponential-

down energy transfer model was applied to treat the collisional stabilization of intermediates, and the parameter $\langle \Delta E_{\mathrm{down}} \rangle$, governing the magnitude of average energy transferred in deactivating collisions with the bath gas particles, was described by a temperature-dependent expression $\langle \Delta E_{\mathrm{down}} \rangle = \Delta E_{\mathrm{down}}^{(0)} (T/T_0)^n$, where $\Delta E_{\mathrm{down}}^{(0)}$ is the value of energy transfer parameter at the standard temperature T_0 = 300 K.

The particular magnitudes of $\Delta E_{\mathrm{down}}^{(0)}$ and n coefficients were chosen in such a way as to correctly describe, within the RRKM-ME formalism, the kinetics of HCO dissociation in N_2 (reported in Ref. [86]) and He (measured in Ref. [87]). More specifically, $\Delta E_{\mathrm{down}}^{(0)}$ was obtained to be 41 cm^{-1} with n = 0.65 for He and 56 cm^{-1} with n = 0.8 for N_2. It should be noted that the very similar energy transfer parameters were adopted in the past for systems with comparable size and atomic composition ($\Delta E_{\mathrm{down}}^{(0)}$ = 80 cm^{-1} and n = 0.85 for a HOCO complex in He [88]; $\Delta E_{\mathrm{down}}^{(0)}$ = 100 cm^{-1} and n = 0.65 for a HOO complex in N_2 [89]; $\Delta E_{\mathrm{down}}^{(0)}$ = 175 cm^{-1} for a C + H_2O system in N_2 [75]; $\Delta E_{\mathrm{down}}^{(0)}$ = 250 ÷ 500 cm^{-1} for CH_3O complex in N_2 [90]). In this study, only N_2 and He were considered since it was for these bath gases that the energy transfer parameters were optimized.

The collision diameter (σ) and the well depth of the Lennard-Jones potential (ε) for intermediates and bath gas particles required for RRKM-ME analysis were estimated using the dipole-reduced formalism method (DRFM) [91] on the basis of computed spatial structures and basic electric properties (*i.e.*, dipole moment and polarizability). It is also worth mentioning that in the course of RRKM-ME calculations, the radiative quenching of vibrationally energized intermediate complexes was ignored because of its minor importance in the RRKM-ME analysis in combustion-related conditions [84,92].

To generate the high-pressure limit rate constants for the barrierless entrance channels, phase space theory [92], as implemented in the MESS package [84-85], was used with an attractive isotropic long-range potential $U = -C_6R^{-6}$. The required values of the potential parameter C_6, in turn, were evaluated within the DRFM framework [91].

Since the R1 reaction is endothermic, it was more reasonable to analyze the rate coefficient for its reverse (-R1 process). In so doing, the -R1 rate constant at P = 1 bar for N_2, as a bath gas, was found by summing over the separate channels and is plotted as a function of temperature, together with the previous results of QCT calculations by Zanchet *et al.* [37] performed in a narrow range of temperatures (below 500 K), in Fig. 4. The -R1 rate constant obtained in this study had a weak nonmonotonic temperature dependence and coincided quite well with the low-temperature predictions made by Zanchet *et al.* [37]. Some discrepancies observed in the absolute rate constant values are not surprising due to the differences in the approaches used and the fact that not all the channels analyzed in the present study were considered in the modeling [37].

Notably, the RRKM-ME calculations in the present study showed that the -R1 (and, equivalently, R1) reaction rate constant did not greatly depend on either pressure (up to 100 bar) or the kind of bath gas. This is also indirectly confirmed by the proximity of the $k_{\text{-R1}}(T)$ dependence estimated in this study to that obtained by Zanchet *et al.* [37] without considering third-body collisions. Therefore, in the range of practically important thermodynamic parameters, the complex-forming nature of $k_{\text{-R1}}(T)$ dependence can be ignored, and this rate constant dependence can be recommended for the future kinetic modeling, as depicted in Fig. 4, irrespective of the pressure and composition of the bath gas. By considering the rate constant of an analogous process toward CO($X^1\Sigma^+$) formation, C + OH → CO($X^1\Sigma^+$) + H (-R0), which we also calculated

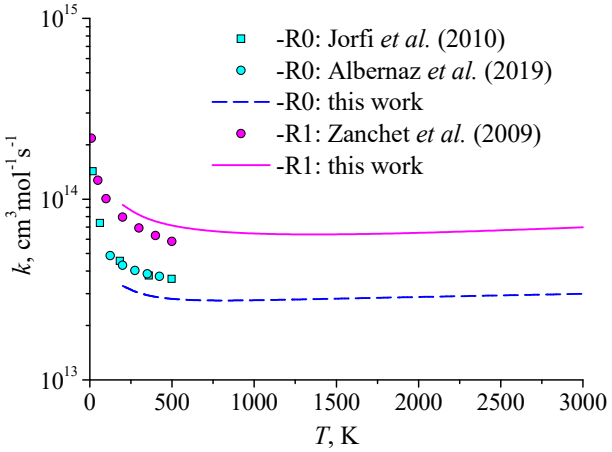

Fig. 4. Thermal rate coefficients for the -R1 and -R0 reaction channels estimated in this study (curves) and reported elsewhere [37,66,68] (symbols).

for N_2 as a bath gas (at $P = 1$ bar) and plotted in Fig. 4 together with the relevant results of QCT modeling by Jorfi *et al.* [66] and RRKM-ME analysis by Albernaz *et al*. [68], one may recognize that while the $k_{-R1}(T)$ and $k_{-R0}(T)$ rate constants differ by about two to three times in magnitude, they similarly depend on temperature. Meanwhile, just as for the -R1 process, there was a slight discrepancy for the -R0 reaction (within 30%) between our estimates and those predicted by other researchers [66,68] due to the differences in the approaches used and the PESs employed.

Likewise, within the RRKM-ME framework, the $k_{R3}(T)$ dependence was estimated, and pressure and diluent gas was found to have no discernable effect on the bimolecular rate constant, as was the case for the -R0 and -R1 reactions. As can be seen in Fig. 5, where the obtained R3 rate constant is depicted, the resulting constant, similar to that of the $k_{-R1}(T)$, is nonmonotonic in temperature. This strongly non-Arrhenius behavior of the $k_{R3}(T)$ dependence is typical for reactions that proceed *via* the pre-reactive complex [93-95]. Indeed, it is not difficult to show that for a reaction path of such type, when the temperature is increased, the bottleneck to the reactive flux moves from the so-called "outer" transition state, associated with a long-range interaction between the colliders, to the "inner" state, associated with the saddle point on the PES), leading to the appearance of a minimum rate constant in the transition region [93].

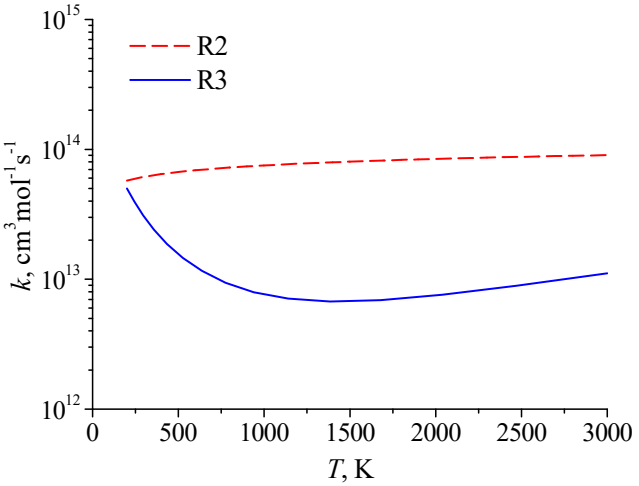

Fig. 5. Thermal rate coefficients for the reaction channels R2 and R3 estimated in this work.

Lastly, the temperature-dependent rate constant of the barrier-free direct bimolecular R2 process was obtained using the capture model, as described in the authors' previous works [60,96]. For this purpose, the required electric properties of CO($a^3\Pi_r$) (dipole moment $\mu = 1.398$ D and static isotropic polarizability $\alpha = 2.451$ Å^3) were borrowed from a previous study [97]. The resulting constant is depicted in Figure 5 against the temperature. As can be expected for a barrierless interaction of a polar particle with a nonpolar one, the desired rate constant had a weak positive temperature dependence: $k_{R2}(T) \sim T^{1/6}$.

For convenience, the calculated temperature-dependent rate constants for -R1, R2, and R3 processes (in cm^3 mol^{-1} s^{-1}) should preferably be fitted over a broad temperature range by a standard three-parameter Arrhenius formula $k(T) = AT^n\exp(-E_a/T)$. However, as can be seen in Fig. 4 and 5, where the obtained rate constants for the -R1 and R3 processes exhibit distinct non-Arrhenius temperature behavior, the $k_{-R1}(T)$ and $k_{R3}(T)$ dependences cannot be approximated by a single Arrhenius expression with reasonable accuracy in the temperature interval under study ($T = 200$-3000 K). Hence, the resulting phenomenological -R1 and R3 reaction rate coefficients were fitted to the double Arrhenius equation. It should be remembered that the pressure dependence of the obtained rate constants was found to be insignificant. As for the R2 thermal rate constant with a plain temperature behavior (Fig. 5), a simple Arrhenius form can obviously be considered appropriate. The respective fitted coefficients obtained in accordance with the above values are given in Table 4.

Table 4. The Obtained Sets of Arrhenius Parameters for the Reactions Under Study

Process	A (cm^3 mol^{-1} s^{-1})	n	E_a, K
-R1[a]	2.139×10^{14}	-0.203	-42.7
	5.778×10^{9}	1.052	-105.9
R2	2.379×10^{13}	0.167	0.0
R3[a]	3.560×10^{17}	-1.606	81.0
	2.105×10^{7}	1.608	-617.1

[a]The rate constant is given as the sum of two Arrhenius expressions.

CONCLUSIONS

This study aimed at conducting *ab initio* quantum chemical calculations using a multireference second-order perturbation theory to comprehensively explore the configuration of the PESs and gain further insight into the reaction kinetics of the $CO(a^3\Pi_r)$ + H, $CO(a^3\Pi_r)$ + H_2, and $CO(a^3\Pi_r)$ + H_2O reacting systems. Accordingly, the key energetically and kinetically favored reaction pathways were identified. It was found that the carbon monoxide molecule excited to the triplet Π state, compared to the ground state CO, reacted more favorably with H, H_2, and H_2O, along the PESs of a basically different configuration, with the heights of the rate-limiting energy barriers being close to zero. In this study, the reactivity of $CO(a^3\Pi_r)$ to these small H-containing species was observed to be extremely high.

In addition, the corresponding reaction rate coefficients were calculated within the RRKM-ME approach or the capture approximation. The RRKM-ME modeling did not reveal an appreciable pressure dependence for rate constants under study, at least in the practically interesting range of thermodynamic parameters. The Arrhenius-type expressions for thermal rate constants were elaborated for a broad temperature range (T = 200-3000 K) relevant to the analysis of CO* chemiluminescence from chemically reacting gas flows. To date, and to the best of our knowledge, there are no available experimental data with which our results for the reaction channels in question can be compared; however, our estimates for the C + OH → $CO(a^3\Pi_r)$ + H channel agree reasonably well with those reported in previous studies. Furthermore, the methodology applied in this work did not account for possible nonadiabatic transitions, which are apparently essential for the processes under study. Thus, the methodology used in this study can provide only a rough idea about the reaction rate constants. Accordingly, the elaborated results are open for future theoretical refinement and, importantly, experimental confirmation.

ACKNOWLEDGEMENTS

This article was prepared as part of the implementation of a program for the creation and development of a world-class scientific center called “The Supersonic” (Sverkhzvuk) for 2020-2025 with financial support from the Ministry of Education and Science of Russia (Agreement No. 075-15-2021-605, dated June 24, 2021).

SUPPLEMENTARY MATERIAL

Supplementary data associated with this article can be found online at http://dx.doi.org/.

REFERENCES

[1] Bell, J. C.; Bradley, D.; Jesch, L. F., Chemi-ionization, chemiluminescence, and electron energy exchange in hydrocarbon-air flames. *Proc. Combust. Inst.* **1971**, *13*, 345-352, DOI: 10.1016/S0082-0784(71)80037-1.

[2] Golde, M. F., Chemiluminescence in gases. *Adv. At. Mol. Phys.*, **1976**, *11*, 361-409, DOI: 10.1016/S0065-2199(08)60034-2.

[3] Kojima, J.; Ikeda, Y.; Nakajima, T., Basic aspects of OH(A), CH(A), and C_2(d) chemiluminescence in the reaction zone of laminar methane–air premixed flames. *Combust. Flame*, 2005, *140*, 34-45, DOI: 10.1016/j.combustflame.2004.10.002.

[4] Zhang, T.; Guo, Q.; Liang, Q.; Dai, Z.; Yu, G., Distribution characteristics of OH*, CH*, and C_2* luminescence in CH_4/O_2 co-flow diffusion flames. *Energy Fuels*, **2012**, *26*, 5503-5508, DOI: 10.1021/ef300970a.

[5] Bedard, M. J.; Fuller, T. L. ; Sardeshmukh, S.; Anderson, W. E., Chemiluminescence as a diagnostic in studying combustion instability in a practical combustor. *Combust. Flame*, **2020**, *213,* 211-225, DOI: 10.1016/j.combustflame.2019.11.039.

[6] Tereza A. M.; Medvedev, S. P. ; Smirnov, V. N., Chemiluminescence of electronically excited species during the self-ignition of acetylene behind reflected shock waves. *Acta Astronaut.*, **2021**, *181*, 612-619, DOI: 10.1016/j.actaastro.2020.09.048.

[7] Kobtsev, V. D.; Kostritsa, S. A.; Pelevkin, A. V.; Smirnov, V. V.; Starik, A. M.; Titova, N. S.; Torokhov, S. A.; Vereshchagin, K. A.; Volkov, S. Y., Ignition and early stage combustion of H_2–O_2 mixture upon the photodissociation of O_2 molecules by UV laser radiation: Experimental and numerical study. *Combust. Flame*, **2019**, *200*, 32-43,

DOI: 10.1016/j.combustflame.2018.10.038.

[8] Chen, X.; Wang, Y.; Zirwes, T.; Zhang, F.; Bockhorn, H.; Chen, Z., Heat release rate markers for highly stretched premixed CH_4/air and CH_4/H_2/air flames. *Energy Fuels*, **2021**, *35*, 13349-13359, DOI: 10.1021/acs.energyfuels.1c02187.

[9] Semenov, N. N. *Some Problems of Chemical Kinetics and Reactivity*. Pergamon: Oxford, **1958**, DOI: 10.1016/C2013-0-06654-6.

[10] Slanger, T.G.; Black, G., CO($a^3\Pi$), its production, detection, deactivation, and radiative lifetime. *J. Chem. Phys.*, **1971**, *55*, 2164-2173, DOI: 10.1063/1.1676387.

[11] Becker, K. H. ; Bayes, K. D., CO chemiluminescence from flames. *J. Chem. Phys.*, **1968**, *48*, 653-661, DOI: 10.1063/1.1668696.

[12] Burke, M. L.; Dimpfl, W. L.; Sheaffer, P. M.; Zittel, P. F.; Bernstein, L. S., Formation of triplet CO in atomic oxygen flames of acetylene and carbon suboxide. *J. Phys. Chem.*, **1996**, *100*, 38-148, DOI: 10.1021/jp950363z.

[13] Fontijn, A.; Goumri, A.; Brock II, P. E., Pressure-dependence of the CO($d^3\Delta$-$a^3\Pi$) triplet bands chemiluminescence intensities from the O + C_2H_2 reaction: mechanistic implications. *Combust. Flame*, **2000**, *121*, 699-701, DOI: 10.1016/S0010-2180(00)00100-0.

[14] Sheaffer, P. M.; Zittel, P. F., UV to near-IR CO emissions from O + C_2H_2 and O + C_3O_2 flames at low pressure and high temperature. *J. Phys. Chem. A*, **2000**, *104*, 10194-10201, DOI: 10.1021/jp001247l.

[15] Vaghjiani, G. L., Investigations of chemiluminescence in the CH_2 + O gas phase reaction. *AIAA paper*, **2001**, *2011*, 3710, DOI:10.2514/6.2001-3710.

[16] Bystrov, N.; Emelianov, A.; Eremin, A.; Loukhovitski, B.; Sharipov, A.; Yatsenko, P., Experimental study of high temperature oxidation of dimethyl ether, n-butanol and methane. *Combust. Flame*, **2020**, *218*, 121-133, DOI: 10.1016/j.combustflame.2020.04.003.

[17] Huber, K. P.; Herzberg, G., *Molecular Spectra and Molecular Structure. Vol. 4. Constants of Diatomic Molecules*. **1979**. Van Nostrand Reinhold, New York.

[18] Wysong, I. J., Measurement of quenching rates of CO($a^3\Pi$, v = 0) using laser pump-and-probe technique. *Chem. Phys. Lett.*, **2000**, *329*, 42-46, DOI: 10.1016/S0009-2614(00)00967-2.

[19] Boubert, P.; Vervisch, P., Laser-induced fluorescence measurements of $a^3\Pi$ metastable carbon monoxide in a high enthalpy flow. *Eur. Phys. J. D*, **2001**, *17*, 43-48, DOI: 10.1007/s100530170035.

[20] Macdonald, R. L.; Munafò, A.; Johnston, C. O.; Panesi, M., State-to-state modeling of CO for Mars entry applications. *AIAA paper*, **2015**, *2015*, 0476, DOI: 10.2514/6.2015-0476.

[21] Macdonald, R. L.; Munafò, A.; Johnston, C. O.; Panesi, M., Nonequilibrium radiation and dissociation of CO molecules in shock-heated flows. *Phys. Rev. Fluids*, **2016**, *1*, 043401, DOI: 10.1103/ PhysRevFluids.1.043401.

[22] McGuire, S. D.; Tibere-Inglesse, A. C.; Mariotto, P. B.; Cruden, B. A.; Laux, C. O., Measurements and modeling of CO 4th positive (A-X) radiation. *J. Quant. Spectrosc. Radiat. Transfer*, **2020**, *245*, 106855, DOI: 10.1016/j.jqsrt.2020.106855.

[23] Melnik, M. Yu.; Kustova, E. V., Impact of electronic excitation on the state-to-state vibrational-chemical CO kinetics. *J. Phys.: Conf. Ser.*, **2022**, *2308*, 012014, DOI: 10.1088/1742-6596/2308/1/012014.

[24] Lomaev, M. I.; Lisenko, A. A.; Tarasenko, V. F., Carbon monoxide emission in VUV spectral region upon excitation of natural gas by a capacitive discharge. *Opt. Spectrosc.*, **2010**, *108*, 923-926, DOI: 10.1134/S0030400X10060147.

[25] Barreto, P. R. P.; de O. Euclides, H.; Albernaz, A. F.; Aquilanti, V.; Capitelli, M.; Grossi, G.; Lombardi, A.; Macheret, S.; Palazzetti, S., Gas phase Boudouard reactions involving singlet-singlet and singlet-triplet CO vibrationally excited states: implications for the non-equilibrium vibrational kinetics of CO/CO_2 plasmas. *Eur. Phys. J. D*, **2017**, *71*, 259, DOI: 10.1140/epjd/e2017-80103-1.

[26] Pietanza, L. D.; Colonna, G.; Laricchiuta, A.; Capitelli, M., Non-equilibrium electron and vibrational distributions under nanosecond repetitively pulsed CO discharges and afterglows: II. The role of radiative and quenching processes. *Plasma Sources Sci. Technol.*, **2018**, 27, 095003, DOI: 10.1088/1361-6595/aad7f2.

[27] Ogloblina, P.; del Caz, A. T.; Guerra, V.; Alves, L. L., Electron impact cross sections for carbon monoxide and

their importance in the electron kinetics of CO_2–CO mixtures. *Plasma Sources Sci. Technol.*, **2020**, *29*, 015002, DOI: 10.1088/1361-6595/ab4e72.

[28] Silva, A. F.; Morillo-Candas, A. S.; del Caz, A. T.; Alves, L. L.; Guaitella, O.; Guerra, V., A reaction mechanism for vibrationally-cold low-pressure CO_2 plasmas. *Plasma Sources Sci. Technol.*, **2021**, *29*, 125020, DOI: 10.1088/1361-6595/abc818.

[29] Silva, T.; Morillo-Candas, A. S.; Guaitella, O.; Guerra, V., Modeling the time evolution of the dissociation fraction in low-pressure CO_2 plasmas. *J. CO_2 Util.*, **2021**, *53*, 101719, DOI: 10.1016/j.jcou.2021.101719.

[30] Pokrovskiy, G. V.; Popov, N. A.; Starikovskaia, S. M., Fast gas heating and kinetics of electronically excited states in a nanosecond capillary discharge in CO_2. *Plasma Sources Sci. Technol.*, **2022**, *31*, 035010, DOI: 10.1088/1361-6595/ac5102.

[31] Arsentiev, I. V., On the influence of discharge parameters on the kinetics of plasma-assisted combustion of synthesis gas in air. *Physical-Chemical Kinetics in Gas Dynamics (in Russian, English abstract)*, **2021**, *22*, DOI: 10.33257/phchgd.22.5.953. URL http://chemphys.edu.ru/issues/2021-22-5/articles/953.

[32] Kirillov, A. S.; Werner, R.; Guineva, V., The influence of metastable molecular nitrogen $N_2(A^3\Sigma_u^+)$ on the electronic kinetics of CO molecules. *Chem. Phys. Lett.*, **2017**, *685*, 95-102, DOI: 10.1016/j.cplett.2017.06.001.

[33] Gérard, J.-C.; Gkouvelis, L.; Ritter, B.; Hubert, B.; Jain, S. K.; Schneider, N. M. MAVEN-IUVS observations of the CO_2^+ UV doublet and CO cameron bands in the Martian thermosphere: Aeronomy, seasonal, and latitudinal distribution. *J. Geophys. Res.: Space Phys.* **2019**, *124*, 5816-5827, DOI: 10.1029/2019JA026596.

[34] Lee, R. A.; Ajello, J. M.; Malone, C. P.; Evans, J. S.; Veibell, V.; Holsclaw, G. M.; McClintock, W. E.; Hoskins, A. C.; Jain, S.; Gerard, J. -C.; Schneider, N. M., Laboratory study of the Cameron bands, the first negative bands and fourth positive bands in the middle ultraviolet 180-280 nm by electron impact upon CO. *J. Geophys. Res.: Planet.*, **2021**, *126*, e2020JE006602, DOI: 10.1029/2020JE006602.

[35] Thirupathaiah, P.; Haider, S. A.; Masoom, J., Simulation of photoelectron flux, electron density, emission rate and limb intensity of CO($a^3\Pi$) Cameron bands in the Martian thermosphere: Comparisons with (1) SPICAM and IUVS observations and (2) other model calculations. *J. Earth Syst. Sci.*, **2022**, *131*, 78, DOI: 10.1007/s12040-022-01822-3.

[36] France, K.; Schindhelm, R. N.; Burgh, E. B.; Herczeg, G. J.; Harper, G. M.; Brown, A.;Green, J. C.; Linsky, J. L.; Yang, H.; Abgrall, H.; Ardila, D.; Bergin, E. A.; Bethell, T. J.; Brown, J. M.; Calvet, N.; Espaillat, C. C.; Gregory, C. C.; Hillenbrand, L. A.; Hussain, G. A. J.; Ingleby, L. D.; Johns-Krull, C. M.; Roueff, È.; Valenti, È.; Walter, F. M., The far-ultraviolet "continuum" in protoplanetary disk systems. II. Carbon monoxide fourth positive emission and absorption. *Astrophys J.*, **2011**, *734*, 31, DOI: 10.1088/0004-637X/734/1/31.

[37] Zanchet, A.; Bussery-Honvault, B.; Jorfi, M.; Honvault, P., Study of the C(^{3}P) + OH($X^2\Pi$) - CO($a^3\Pi$) + H(^{2}S) reaction: fully global ab initio potential energy surfaces of the 1^2A'' and 1^4A'' excited states and non adiabatic couplings. *Phys. Chem. Chem. Phys.*, **2009**, *11*, 6182-6191, DOI: 10.1039/b903829a.

[38] Zanchet, A.; Gonzalez-Lezana, T.; Roncero, O.; Jorfi, M.; Honvault, P.; Hankel, M., An accurate study of the dynamics of the C+OH reaction on the second excited 1^4A'' potential energy surface. *J. Chem. Phys.*, **2012**, *136*, 164309, DOI: 10.1063/1.4705426.

[39] Jorfi, M.; Gonzalez-Lezana, T.; Zanchet, A. ; Honvault, P.; Bussery-Honvault, B., Quasiclassical trajectory and statistical quantum calculations for the C + OH → CO + H reaction on the first excited 1^2A'' potential energy surface. *J. Phys. Chem. A*, **2013**, *117*, 1872-1879, DOI: 10.1021/jp309764g.

[40] Keshavarz, F.; Mousavipour, H., A single- and multireference study on CH($X^2\Pi$) reaction with $O_2(X^3\Sigma_g^-)$. *Int. J. Chem. Kinet.*, **2019**, *51*, 161-177, DOI: 10.1002/kin.21240.

[41] DeVine, J. A.; Choudhury, A.; Lau, J. A.; Schwarzer, D.; Wodtke, A. M., Spin-Forbidden Carbon-Carbon Bond Formation in Vibrationally Excited α-CO. *J. Phys. Chem. A*, **2022**, 126, 2270-2277, DOI: 10.1021/acs.jpca.2c01168.

[42] Dawes, R.; Ndengué, S.A., Single- and multireference electronic structure calculations for constructing potential energy surfaces. *Int. Rev. Phys. Chem.*, **2016**,

35, 441-478, DOI: 10.1080/0144235X.2016.1195102.

[43] Freidzon, A.; Tsybizova, A., CASSCF and Firefly: A tutorial (accessed may 2022), **2017**. URL https://www.researchgate.net/publication/317106028.

[44] Yin, H.-M.; Kable, S. H.; Zhang, X.; Bowman, J. M., Signatures of H_2CO Photodissociation from Two Electronic States, *Science*, **2006**, *311*, 1443-1446, DOI: 10.1126/science.1123397.

[45] Park, J. W.; Al-Saadon, R.; MacLeod, M. K.; Shiozaki, T.; Vlaisavljevich, B., Multireference electron correlation methods: Journeys along potential energy surfaces. *Chem. Rev.*, **2020**, *120*, 5878-5909, DOI: 10.1021/acs.chemrev.9b00496.

[46] Asemani, S. S.; Mousavipour, S. H., Dynamics of imidogen reaction with hydroxyl radical: a theoretical approach. *J. Iran. Chem. Soc.*, **2020**, *17*, 1987-2000, DOI: 10.1007/s13738-020-01905-2.

[47] Yazdanpanahfard, Z.; Oftadeh, M.; Fakhraee, S., Ultrafast luminescence decay in Rhenium(I) complexes with Imidazo[4,5-f]-1,10-phenanthroline ligands: TDDFT method. *Phys. Chem. Res.*, **2020**, *8*, 609-627, DOI: 10.22036/pcr.2020.210913.1705.

[48] Roos, B. O., The complete active space self-consistent field method and its applications in electronic structure calculations. In Lawley, K. P., editor, *Advances in Chemical Physics: Ab Initio Methods in Quantum Chemistry Part 2*, volume 69. John Wiley & Sons, Inc., Hoboken, NJ, USA., **1987**. DOI: 10.1002/9780470142943.ch7.

[49] Schmidt, M. W.; Gordon, M. S., The construction and interpretation of MCSCF wavefunctions. *Annu. Rev. Phys. Chem.*, **1998**, *49*, 233-266, DOI: 10.1146/ annurev.physchem.49.1.233.

[50] Granovsky, A. A., Extended multi-configuration quasi-degenerate perturbation theory: The new approach to multi-state multi-reference perturbation theory. *J. Chem. Phys.*, **2011**, *134*, 214113, DOI: 10.1063/ 1.3596699.

[51] Bertran, J., Some fundamental questions in chemical reactivity. *Theor. Chem. Acc.*, **1998**, *99*, 143-150, DOI: 10.1007/s002140050316.

[52] Pascual, R. Z.; Schatz, G. C.; Lendvay, G.; Troya, G., Quasiclassical trajectory and transition state theory studies of the N(^{4}S) + H2 ↔ NH($X^3\Sigma^-$) + H reaction. *J. Phys. Chem. A*, **2002**, *106*, 4125-4136, DOI: 10.1021/jp0133079.

[53] Harding, L. B.; Klippenstein, S. J.; Jasper, A. W., Ab initio methods for reactive potential surfaces. *Phys. Chem. Chem. Phys.*, **2007**, *9*, 4055-4070, DOI: 10.1039/b705390h.

[54] Fracchia, F.; Cimiraglia, R.; Angeli, C., Assessment of multireference perturbation methods for chemical reaction barrier heights. *J. Phys. Chem. A*, **2015**, *119*, 5490-5495, DOI: 10.1021/jp512669z.

[55] Monge-Palacios, M.; Rafatijo, H., On the role of the termolecular reactions $2O_2 + H_2 \rightarrow 2HO_2$ and $2O_2 + H_2 \rightarrow H + HO_2 + O_2$ in formation of the first radicals in hydrogen combustion: *ab initio* predictions of energy barriers. *Phys. Chem. Chem. Phys.*, **2017**, *19*, 2175-2185, DOI: 10.1039/c6cp07029a.

[56] Hassani, N.; Mousavipour, H. S.; Mohajeri, A., Kinetics and mechanism of the NH($X^3\Sigma^-$) + SO($X^3\Sigma^-$) reaction: A theoretical approach. *J. Phys. Chem. A*, **2000**, *124*, 6585-6600, DOI: 10.1021/acs.jpca.0c01950.

[57] Budzák, Š.; Scalmani, G.; Jacquemin, D., Accurate excited-state geometries: a CASPT2 and coupled-cluster reference database for small molecules. *J. Chem. Theory Comput.*, **2017**, *13*, 6237-6252, DOI: 10.1021/acs.jctc.7b00921.

[58] Veryazov, V.; Malmqvist, P. A.; Roos, B. O., How to select active space for multiconfigurational quantum chemistry? *Int. J. Quantum Chem.*, **2011**, *111*, 3329-3338, DOI: 10.1002/qua.23068.

[59] Kendall, R. A.; Dunning Jr., T. H.; Harrison, R. J., Electron affinities of the first-row atoms revisited. Systematic basis sets and wave functions. *J. Chem. Phys.*, **1992**, *96*, 6796-6806, DOI: 10.1063/1.462569.

[60] Pelevkin, A. V.; Sharipov, A. S., Reactions of electronically excited molecular nitrogen with H_2 and H_2O molecules: Theoretical study. *J. Phys. D: Appl. Phys.*, **2018**, *51*, 184003, DOI: 10.1088/1361-6463/aab97f.

[61] Minaev, B. F.; Panchenko, A. A., New aspects of the airglow problem and reactivity of the dioxygen quintet $O_2(^5\Pi_g)$ state in the MLT region as predicted by DFT calculations. *J. Phys. Chem. A*, **2020**, *124*, 9638-9655, DOI: 10.1021/acs.jpca.0c07310.

[62] Granovsky, A. A., Firefly V. 8.2.0 (accessed jan 2019).

URL http://classic.chem.msu.su/gran/firefly/index.html.

[63] Schmidt, M. W.; Baldridge, K. K.; Boatz, J. A.; Elbert, S. T.; Gordon, M. S., Jensen, J. H.;Koseki, S.; Matsunaga, N.; Nguyen, K. A.; Su, S.; Windus, T. L.; Dupuis, M.; Montgomery, J. A., General atomic and molecular electronic structure system. *J. Comput. Chem.*, **1993**, *14*, 1347-1363, DOI: 10.1002/jcc.540141112.

[64] Gonzalez, C.; Schlegel, B. H., An improved algorithm for reaction path following. *J. Chem. Phys.*, **1989**, *90*, 2154-2162, DOI: 10.1063/1.456010.

[65] Bruna, P. J.; Buenker, R. J.; Peyerimhoff, S. D., *Ab initio* study of the structure, isomers and vertical electronic spectrum of the formyl radical HCO. *J. Mol. Struct.*, **1976**, *32*, 217-233, DOI: 10.1016/0022-2860(76)85001-6.

[66] Jorfi, M. ; Bussery-Honvault, B.; Honvault, P.; Stoecklin, T.; Larrégaray, P.; Halvick, P., Theoretical sensitivity of the $C(^3P)$ + $OH(X^2\Pi)$ → $CO(X^1\Sigma^+)$ + $H(^2S)$ rate constant: The role of the long-range potential. *J. Phys. Chem. A*, **2010**, *114*, 7494-7499, DOI: 10.1021/jp1037377.

[67] Peters, P. S.; Duflot, D.; Wiesenfeld, L.; Toubin, C., The H + CO = HCO reaction studied by ab initio benchmark calculations. *J. Chem. Phys.*, **2013**, *139*, 164310, DOI: 10.1063/1.4826171.

[68] Albernaz, A. F.; da Silva, W. B.; Barreto, P. R. P.; Correa, E., Thermal rate constant for the $C(^3P)$ + $OH(X^2\Pi)$ → $CO(X^1\Sigma)$ + $H(^2S)$ reaction using stochastic energy grained master equation. *Int. J. Chem. Kinet.*, **2019**, *51*, 590-601, DOI: 10.1002/kin.21279.

[69] Vichietti, R. M.; Machado, F. B. C.; Haiduke, R. L. A., Accurate rate constants for the forward and reverse H + CO ↔ HCO reactions at the high-pressure limit. *ACS Omega*, **2020**, *5*, 23975-23982, DOI: 10.1021/acsomega.0c03267.

[70] Chen, Q.; Han, S.; Hu, X.; Xie, D. , Full-dimensional potential energy surfaces of ground (X^2A') and excited (A^2A'') electronic states of HCO and absorption spectrum. *Chin. J. Chem. Phys.*, **2022**, *35*, 303-310, DOI: 10.1063/1674-0068/cjcp2112270.

[71] Ruscic, B.; Bross, H., Active thermochemical tables (ATcT) values based on ver. 1.122 of the thermochemical network (accessed may 2022), **2016**. URL https://atct.anl.gov/.

[72] Zhang, X.; Zou, S.; Harding, L. B. ; Bowman, J. M., A global *ab initio* potential energy surface for formaldehyde. *J. Phys. Chem. A*, **2004**, *108*, 8980-8986, DOI: 10.1021/jp048339l.

[73] Wang, X.; Houston, P. L.; Bowman, J. M., A new (multi-reference configuration interaction) potential energy surface for H_2CO and preliminary studies of roaming. *Phil. Trans. R. Soc. A*, **2017**, *375*, 20160194, DOI: 10.1098/rsta.2016.0194.

[74] Lee, K. L. K.; Quinn, M. S.; Kolmann, S. J.; Kable, S. H.; Jordan, M. J. T., Zero-point energy conservation in classical trajectory simulations: Application to HCO. *J. Chem. Phys.*, **2018**, *148*, 194113, DOI: 10.1063/1.5023508.

[75] Keshavarz, F., Chemical kinetics approves the occurrence of $C(^3P_j)$ reaction with H_2O. *J. Phys. Chem. A*, **2019**, *123*, 5877-5892, DOI: 10.1021/acs.jpca.9b03492.

[76] Jacox, M. E., Vibrational and electronic energy levels of polyatomic transient molecules. Supplement B. *J. Phys. Chem. Ref. Data*, **2003**, *32*, 1-437, DOI: 10.1063/1.1497629.

[77] de Albuquerque Martins, L. M. M.; Arbilla, G.; da Silva, E. C., Unimolecular decomposition of formaldehyde: H_2CO → H_2 + CO. Part I: *Ab initio* reaction path and variational transition state rate constants. *J. Phys. Chem. A*, **1998**, *102*, 10805-10812, DOI: 10.1021/jp982962m.

[78] Hu S. -W.; Lu, S. -M.; Wang, X. -Y., Theoretical investigation of gas-phase thermal reactions between carbon monoxide and water. *J. Phys. Chem. A*, **2004**, *108*, 8485-8494, DOI: 10.1021/jp047486g.

[79] Döntgen, M.; Leonhard, K., Reactions of chemically activated formic acid formed *via* HCO + OH. *J. Phys. Chem. A*, **2016**, *120*, 1819-1824, DOI: 10.1021/acs.jpca.6b00887.

[80] Vichietti, R. M.; Spada, R. F. K.; da Silva, A. B. F.; Machado, F. B. C.; Haiduke, R. L. A., Accurate calculations of rate constants for the forward and reverse H_2O + CO → HCOOH reactions. *Chem. Select*, **2017**, *2*, 7267-7272, DOI: 10.1002/slct.201701137.

[81] Armentrout, P. B., Chemistry of excited electronic

states. *Science*, **1991**, *251*, 175-179, DOI: 10.1126/science.251.4990.175.

[82] Miller, J. A.; Klippenstein, S. J., Master equation methods in gas phase chemical kinetics. *J. Phys. Chem. A*, **2006**, *110*, 10528-10544, DOI: 10.1021/jp062693x.

[83] Klippenstein, S. J., From theoretical reaction dynamics to chemical modeling of combustion. *Proc. Combust. Inst.*, **2017**, *36*, 77-111, DOI: 10.1016/j.proci.2016.07.100.

[84] Georgievskii, Y.; Miller, J. A.; Burke, M. P.; Klippenstein, S. J., Reformulation and solution of the master equation for multiple-well chemical reactions. *J. Phys. Chem. A*, **2013**, *1170*, 12146-12154, DOI: 10.1021/jp4060704.

[85] Georgievskii, Y.; Klippenstein, S. J., Master equation system solver MESS.2016.3.23. Available at: http://tcg.cse.anl.gov/papr/codes/mess.html.

[86] Li, J.; Zhao, Z.; Kazakov, A.; Chaos, M.; Dryer, F. L.; Scire, J. J., A comprehensive kinetic mechanism for CO, CH_2O, and CH_3OH combustion. *Int. J. Chem. Kinet.*, **2007**, *39*, 109-136, DOI: 10.1002/kin.20218 .

[87] Krasnoperov, L. N.; Chesnokov, E. N.; Stark, H.; Ravishankara, A. R., Unimolecular dissociation of formyl radical, HCO → H + CO, studied over 1-100 bar pressure range. *J. Phys. Chem. A*, **2004**, *108*, 11526-11536, DOI: 10.1021/jp0403994.

[88] Senosiain, J. P.; Klippenstein, S. J.; Miller, J. A., A complete statistical analysis of the reaction between OH and CO. *Proc. Combust. Inst.*, **2005**, *30*, 945-953, DOI: 10.1016/j.proci.2004.07.009.

[89] Sellevag, S. R.; Georgievskii, Yu.; Miller, J. A., The temperature and pressure dependence of the reactions H + O_2(+M) → HO_2(+M) and H + OH(+M) → H_2O(+M). *J. Phys. Chem. A*, **2008**, *112*, 5085-5095, DOI: 10.1021/jp711800z.

[90] Mousavi, S.; Mousavipour, S. H., A theoretical study on the dynamics of gas-phase reaction of methyl cation with atomic oxygen. *J. Iran. Chem. Soc.*, **2019**, *16*, 807-825, DOI: 10.1007/s13738-018-1558-x.

[91] Paul, P.; Warnatz, J., A re-evaluation of the means used to calculate transport properties of reacting flows. *Proc. Combust. Inst.*, **1998**, *27*, 495-504, DOI: 10.1016/S0082-0784(98)80439-6.

[92] Fernandez-Ramos, A.; Miller, J. A.; Klippenstein, S. J.; Truhlar, D. G., Modeling the kinetics of bimolecular reactions. *Chem. Rev.*, **2006**, *106*, 4518-4584, DOI: 10.1021/cr050205w.

[93] Greenwald, E. E.; North, S. W.; Georgievskii, Y.; Klippenstein, S. J., A two transition state model for radical-molecule reactions: a case study of the addition of OH to C_2H_4. *J. Phys. Chem. A*, **2005**, *109*, 6031-6044, DOI: 10.1021/JP058041A.

[94] Nguyen, T. L.; Stanton, J. F., *Ab initio* thermal rate calculations of HO + HO = O(^{3}P) + H_2O reaction and isotopologues. *J. Phys. Chem. A*, **2013**, *117*, 2678-2686, DOI: 10.1021/jp312246q.

[95] Saheb, V.; Nazari, A., Products of the self-reaction of HCO radicals: Theoretical kinetics studies. *Phys. Chem. Res.*, **2019**, *7*, 81-94, DOI: 10.22036/pcr.2018.149431.1540.

[96] Sharipov, A. S.; Starik, A. M., Theoretical study of the reactions of ethanol with aluminum and aluminum oxide. *J. Phys. Chem. A*, **2015**, *119*, 3897-3904, DOI: 10.1021/acs.jpca.5b01718.

[97] Sharipov, A.; Loukhovitski, B.; Pelevkin, A., Diffusion coefficients of electronically excited molecules. *Physical-Chemical Kinetics in Gas Dynamics (in Russian, English abstract)*, **2021**, *22*, DOI: 10.33257/phchgd.22.1.913 . URL http://chemphys.edu.ru/issues/2021-22-1/articles/913/.